Comput Mech (2008) 42:607–618
DOI 10.1007/s00466-008-0247-5

ORIGINAL PAPER

Atomistic-based continuum constitutive relation for microtubules: elastic modulus prediction

Hanqing Jiang · Liying Jiang · Jonathan D. Posner · Bryan D. Vogt

Received: 20 August 2007 / Accepted: 18 January 2008 / Published online: 12 February 2008

Abstract Mechanical behavior of cells is primarily governed by the cytoskeleton (CSK), a remarkable system of filaments consisting of microtubules, actin filaments and intermediate filaments. This system defines the shape and bulk mechanical properties of the cell. In order to understand how the CSK network influences the mechanical behavior of living cells from a theoretical perspective, the mechanical properties of an individual CSK filament must first be properly described. Existing atomistic simulation methods have computational size limitations; conversely, conventional continuum mechanics lack fundamental nanoscale information. Here a new simulation method is developed that bridges the gap between these two simulation regimes using an atomistic-based continuum constitutive relation for microtubules based on the interatomic potential for proteins and specific atomic structures. This theory is used to predict the elastic modulus of microtubules, which agrees with the range of experimentally measured values without any parameter fitting. The proposed method is applicable to other biopolymers if the subunits are bonded through noncovalent bonds.

H. Jiang (✉) · J. D. Posner
Department of Mechanical and Aerospace Engineering,
Arizona State University,
Tempe, AZ 85287, USA
e-mail: hanqing.jiang@asu.edu

L. Jiang
Department of Mechanical and Materials Engineering,
University of Western Ontario,
London, ON N6A 5B9, Canada

B. D. Vogt
Department of Chemical Engineering,
Arizona State University,
Tempe, AZ 85287, USA

Keywords Microtubules · Atomistic-based · Continuum constitutive relation

1 Introduction

The ability of a cell to sustain mechanical loads originates from cellular components serving as mechanical load bearing members. Among these components, the cytoskeleton (CSK), a system of filaments, primarily governs the mechanical behavior of cells (e.g., [1]). The CSK is a dynamic, living structure that defines the cell's shape and bulk mechanical properties. Many cellular functions such as gene expression, cell division, motility, signal transduction, wound healing and apoptosis (programmed cell death) are mediated by the physical properties of CSK. Changes in the viscoelastic properties of living cells have been used as biomarkers for disease and invasion by foreign organisms [2,3]. For example, cancer metastasis occurs when sessile cells in a tumor migrate and invade nearby tissues which depend on the mechanical properties of the cell. Thus, fundamental understanding of the mechanical properties of cells could provide a route to disease diagnosis; the CSK network is the most important member to this end and fundamental understanding of the mechanical properties of this network is the focus of this paper.

CSK consists of three major filamentous biopolymers: microtubules, actin filaments and intermediate filaments. Each type of filament has distinct mechanical properties, resultant from different protein subunits and nanoscale structure. A microtubule is a long, hollow cylindrical tube comprised of tubulin protein, a dimer formed from two globular proteins (α-tubulin and β-tubulin). Microtubules are usually considered to carry compressive forces as they resist con-

traction (e.g., [4]). Actin filaments are composed of double stranded helical polymers and relatively flexible compared with the hollow cylindrical microtubules. Primary role of actin filaments is to carry tensile forces (e.g., [5]). An intermediate filament is a ropelike fiber comprised by 32-individual α-helical monomer [1]. The role of intermediate filament network in living cells is less understood than that for the other filaments. Intermediate filaments are presumed to be responsible for carrying tensile force, but only at relatively large applied strains ($>20\%$) when their contribution to the cell's rigidity becomes significant [6].

Since the mechanical behavior of cells is primarily controlled by CSK, proper description of the mechanical properties of individual CSK filaments is an important start to understand the intricacies of the CSK network. Most existing studies of CSK filaments focus on the experimental measurements in vitro. Multiple techniques have been used to characterize the mechanical properties of filaments including cone and plate rheometry (e.g., [7,8]), optical trapping/buckling [9,10], vesicle rupturing from in situ polymerization [11–13], atomic force microscopy [14,15], and particle tracking microrheology [16]. One issue for these measurements is the lack of agreement between techniques because different assumptions are necessary to analyze the measured data in terms of mechanical properties of the individual microtubules or actin filaments. For example, Wagner et al. [17] measured the elastic modulus of microtubules gels about 2.29–2.55 GPa. This measurement provides the ensemble average of the mechanical properties of microtubules, but also may include the contributions from the water present in the gel as well. Thus, these measurements may not accurately describe the mechanical properties of individual microtubules. Conversely, de Pablo et al. [18] observed only 1 GPa for the modulus of individual microtubules measured using a scanning force microscope (SFM) technique. In this case, individual microtubules were probed, but the data interpretation is significantly more difficult. de Pablo et al. [18] modeled the microtubules by classical shell theory that is established based on collective behavior of a great deal of atoms. The applicability of classical shell theory down to nanoscale is somewhat unclear. Additionally, as clearly pointed out by de Pablo et al., the elastic modulus of individual microtubules strongly depends on the choice of "shell thickness" since the microtubule is not a shell with uniform thickness but has deep grooves between the protofilaments. The elastic modulus of individual microtubules varies from 0.4 to 2.0 GPa as the assumed shell thickness varies between 2.4 and 1.1 nm. Since it is unclear how the macroscopic gel modulus relates to the individual microtubule and equal difficult is encountered in the interpretation of the SFM measurement of the mechanics of individual microtubules, it is unclear what measurement provides a more physically accurate modulus for individual microtubules. There is significant variability in the mechanical properties depending upon experimental technique utilized and assumptions of the shell thickness. The development of a physically realistic atomic-based model for these filaments should be able to lend guidance to the design of experimental methods for determining the mechanical properties of individual CSK filaments.

Parallel to these direct and indirect experimental measurements, there have been some theoretical attempts to study the mechanical properties of CSK. These theoretical studies have the potential to identify phenomena not easily accessible by experiments and can be divided into two categories, atomistic simulations, such as molecular dynamics (MD) simulations, and continuum modeling. MD simulations accurately capture the all-atom force fields and interactions between atoms/molecules and are therefore suitable for detailed studies of biomolecules. There also exist widely used MD simulations programs, such as CHARMM [19] and AMBER [20] for biomolecules. However to date, MD simulations focus on proteins (e.g., [21,22]), not filaments, because the maximum size that MD simulations can reach is on the order of 10^6 atoms (or a cube of 50 nm^3) [23] while the characteristic length of an individual filament is on the order of 100 nm with a complex structure. For example, the subunit of microtubule, tubulin protein (Protein Data Bank (www.pdb.org) Id: 1TUB) has 440 residues consisting of about 8,000 atoms, and the subunit of actin filament, actin protein (PDB ID: 1J6Z) has 376 residues consisting of about 7,000 atoms. In order to study the mechanical properties of an individual CSK filament, one has to consider at least hundreds of subunits, i.e., about 10^6 atoms for an individual CSK filament. To simulate a CSK network consisting of many filaments to determine the mechanical behavior of living cells, the number of atoms (up to 10^8–10^9 atoms) is computationally prohibited for MD simulations.

To manage the large number of atoms, coarse-grained model have been developed that have reduced degrees of freedom and eliminate some of the fine interaction details by constructing coarse-grained mesh. Coarse-grained model can study larger system compared with all-atom MD simulations and have been applied in a limited manner to CSK [23,24]. Although coarse-grained model can overcome some of the length scale limitations, this method is still limited by the inherent time scale (10^{-9}–10^{-6} s) of MD simulations, which makes it unsuitable to study many cellular behaviors: for example, CSK reorganization on the order of minutes [25].

An alternative method for modeling CSK is to start at the macroscale continuum modeling efforts [26]. Most researchers model CSK as linear/nonlinear elastic/viscoelastic solid. Each filament is typically modeled as a relatively simple object with idealized structural geometry made up of an isotropic, homogeneous, and elastic material [27–29]. One major advance obtained with continuum mechanics is the concept of

"tensegrity" [5] (tensional integrity) where actin filaments and microtubules are modeled as pre-stressed cables and compression-bearing struts, respectively (e.g., [30,31]). For a more realistic representation, some researchers attempted to model CSK network as a viscoelastic solid [32,33]. These models are phenomenological and do not include the atomistic details of the proteins subunits. Thus, a continuum description of CSK from atomistic interactions is important to fundamental understanding of CSK mechanics. Boey et al. [34] modeled CSK as a polymer chain that is characterized by the potential $V(r)$ consisting of repulsive and attractive terms. However, the parameters in the potential are simply fitting and not based on atomic-scale structures. These methods therefore cannot relate the atomic-scale structures to macro-scale mechanical properties nor enable correlation of the macro-scale mechanical properties to the health of living cells.

There exists a large gap between atomic-scale simulations of individual monomers and continuum modeling of CSK network. A universal description from the finest components (proteins) at nanoscale to the entire cell at the microscale is necessary. Therefore, it is critical that a multiscale simulation method is developed for understanding of cellular behavior to complement and lend insight to experimental studies. There are some attempts to establish atomistic-based continuum theories or hybrid atomistic/continuum theories. Among many efforts in atomistic-based continuum theories, a few examples are as follows. For example, Tadmor et al. [35,36], Miller et al. [37] and Shenoy et al. [38,39] proposed a quasi-continuum model to link atomistic simulation with continuum analysis. Friesecke and James [40] proposed an approach to pass the atomistic information to a continuum theory for a nanostructure in which one or more dimensions are large relative to atomic scale. Arroyo and Belytschko [41] developed an atomistic-based continuum theory for nanoscale membranes. Xiao and Yang [42,43] developed a temperature-related Cauchy-Born rule for crystalline solids. Chung and Narnburu [44] proposed a framework involving atoms and continuums. Jiang and co-workers [45–47] have developed an approach to incorporate the interatomic potential for carbon into a continuum model for carbon nanotubes.

In this paper, we develop an atomistic-based continuum constitutive relation for biopolymers and take the microtubules as an example. The elastic modulus, bending rigidity and stress-strain relations for microtubules are calculated. In Sect. 2, the atomistic potential for proteins [48] will be introduced. The atomistic structure of microtubules will be discussed in Sect. 3. We present an atomistic-based continuum constitutive relation based on the interatomic potential and the structure, and use the proposed theory to calculate the elastic modulus of microtubules in Sect. 4. The applicability and limitation of the proposed theory are discussed in Sect. 5.

2 Interatomic potential for proteins

Here we adopt the interatomic potential for proteins (also 95 AMBER potential) given by Cornell et al. [48] as

$$\begin{aligned} E_{\text{tot}} &= E_{\text{bonded}} + E_{\text{non-bonded}} \\ &= \sum_{\text{bond}} K_r \left(r - r_{\text{eq}}\right)^2 + \sum_{\text{angles}} K_\theta \left(\theta - \theta_{\text{eq}}\right)^2 \\ &\quad + \sum_{\text{dihedrals}} \frac{V_n}{2}\left[1 + \cos\left(n\phi - \gamma\right)\right] \\ &\quad + \sum_{i<j} 4\varepsilon_{ij}\left(\frac{\sigma_{ij}^{12}}{r_{ij}^{12}} - \frac{\sigma_{ij}^{6}}{r_{ij}^{6}}\right) + \sum_{i<j} \frac{q_i q_j}{D R_{ij}}. \end{aligned} \tag{1}$$

The total interatomic potential depends on the atomic positions of all atoms in the system and is the summation of bonded energies E_{bonded} and non-bonded energies $E_{\text{non-bonded}}$. The bonded energies E_{bonded} describe the energies related to the covalent bonds and consist of three contributions from bond stretching, bond bending, and torsional angle. The bond stretching energy $\sum_{\text{bond}} K_r \left(r - r_{\text{eq}}\right)^2$ is a harmonic energy representing the interaction between a pair of atoms which are separated by one covalent bond with bond length r. The force constant K_r determines the strength of the covalent bond and r_{eq} is the equilibrium bond length. The bond bending energy also takes harmonic form. K_θ is the bending force constant and θ_{eq} is the equilibrium angle. The torsional angle energy $\sum_{\text{dihedrals}} \frac{V_n}{2}\left[1 + \cos\left(n\phi - \gamma\right)\right]$ is raised from the steric barriers between atoms separated by 3 covalent bonds and is expressed by a dihedral angle ϕ, where V_n the height of the torsional barrier, n the number of maxima (or minima) in one full rotation and γ describes the angular offset. All three energies are related to the covalent bonds in the system. The energies for non-bonded interactions have two components: the van der Waals interaction (which implicitly includes hydrogen bonds as will be discussed) and the electrostatic interaction. The van der Waals interaction is modeled as the Lennard–Jones 6–12 potential with atom-type dependent constants ε_{ij} and σ_{ij}, which denote the well depth and the separation of atoms i and j where the van der Waals interaction equates zero. The electrostatic interactions are expressed by Coulomb potential, where D is the effective dielectric constant for the media and r_{ij} is the distance between two atoms with charge q_i and q_j. Remarkably, in this widely accepted atomistic potential for protein, there is *no specific function for hydrogen bonds since they have been included in the van der Waals interactions* as justified by Cornell et al. [48]. For the purpose of clarification, we will use the term non-covalent bonds instead of van der Waals interactions in the following since this van der Waals interactions term includes both conventional van der Waals interactions and hydrogen bonds. In the follow-

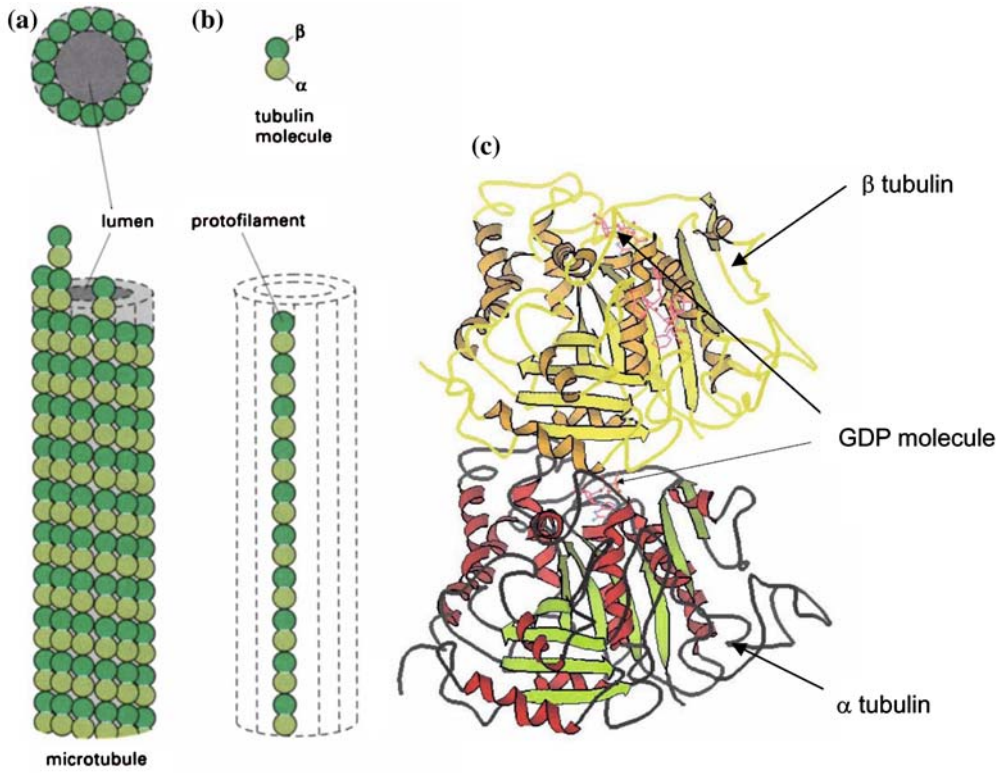

Fig. 1 The structure of a microtubule and its subunit. **a** A microtubule is a hollow, cylindrical tube formed from 13 protofilaments aligned in parallel. **b** One tubulin subunit ($\alpha - \beta$ heterodimers) and one protofilament. **c** Structure of $\alpha - \beta$ heterodimers, tightly bonded by GDP molecule through noncovalent bonds (van der Waals interactions) [1]

ing analysis, we ignore the electrostatic potential as to be discussed in Sect. 4.1.

The parameters for these terms, such as K_r, K_θ, V_n, are determined from studies of small model compounds and comparisons to the geometry and vibrational spectra and depend on specific atom types. The detailed data for different types of atoms were tabulated by Cornell et al. [48] and applied here to the model.

3 Atomic structures of microtubules

A microtubule is a long, hollow, cylindrical tube, typically formed by 13 protofilaments that are aligned in parallel (Fig. 1a). There also exist some microtubules with 14 or 15 protofilaments, especially for microtubules assembled in vitro [49]. The current study is focused on the microtubules with 13 protofilaments since they are the majority in vivo. Each protofilament consists of many bonded α- and β-tubulin monomers (Fig. 1b). Each α or β monomer has a binding site for one guanosine triphosphate (GTP) or guanosine diphosphate (GDP) molecule, i.e., two monomers are connected by a GTP (or GDP) molecule through *noncovalent bonds*, confirmed by the analysis of atomic structure [1]. When the tubulin heterodimers assemble to form the protofilament, a new interface between two tubulins is generated, which is very similar to the interface holding the α- and β-tubulin monomers together by GTP (or GDP) molecule [1]. Therefore, an individual protofilament can be considered as many pairs of α- and β-tubulin monomers that are connected in series by GDP binding sites through noncovalent bonds. The atomic structure of tubulin protein can be obtained in Protein Data Bank with protein ID 1TUB. Figure 1c shows the atomic structure of $\alpha - \beta$ heterodimers, in which α- and β-tubulin monomers are tightly bonded by GDP molecule through noncovalent bonds. We use this structure as the basis for our model.

4 Microtubules continuum constitutive relation based on interatomic potential

4.1 Continuum constitutive relation

Each α- or β-tubulin has a complicated atomic structure shown in Fig. 1c, including α-helix and β-sheets. Interatomic energy is characterized by bonded energy via covalent bonds and non-bonded energy (including van der Waals interactions and hydrogen bonds) given by Eq. 1. Bonded energy is the leading term for each monomer since covalent bond energy is

much stronger than non-bonded energy. The same situation also holds for GDP molecule, i.e., the bonded energy dominates. For a $\alpha-\beta$ heterodimer, the interface is characterized by non-bonded energy.

Given the geometrical characteristics of the protofilament shown in Fig. 1b, a protofilament is modeled as a one-dimensional atomic chain with periodic molecular bases, namely: α-tubulin, GDP molecule, β-tubulin and GDP molecule. Each of the individual four molecules is held together by strong covalent bonds while they are interconnected by weaker non-covalent bonds. Thus most of the deformation occurs at the relatively weak interface, not in the stiff biomolecules. We therefore assume that each tubulin monomer is a rigid body with negligible deformation in comparison to the relatively large deformation at the weak interface. There are four loading conditions for a shaft or tube (e.g., microtubules), namely, axial loading (tension/compression), torsional loading, bending, and shear. All of these loading conditions result in direct (or indirect) tension/compression at the molecular level and thus the overall behavior of a microtubule is primarily controlled by the weak interface.

As illustrated in Fig. 2, we model the protofilament as a one-dimensional chain that consists of rigid bodies connected with non-linear springs. The rigid bodies represent periodic α-tubulin, β-tubulin, and GDP molecule and the non-linear springs denote the interfaces between rigid bodies. Therefore, the overall mechanical behavior is governed by the interfacial behavior, which is the so-called cohesive law. The interface is characterized by non-bonded energy $U\left(r_{ij}\right)$, provided by Cornell et al. [48] in Lennard-Jones form

$$U\left(r_{ij}\right)=4\varepsilon_{ij}\left(\frac{\sigma_{ij}^{12}}{r_{ij}^{12}}-\frac{\sigma_{ij}^{6}}{r_{ij}^{6}}\right). \tag{2}$$

For specific atoms, such as carbon (C) and oxygen (O), Cornell et al. [48] tabulated the parameters for ε_{ij} and σ_{ij}. By summarizing the contributions from all atoms, the cohesive stress will be obtained.

Even we ignore the deformation of tubulins and GDP molecules; the interaction between GDP molecule and tubulins is still very complicated since they have thousands of atoms. In order to establish a continuum description of the interface rather than tracking each individual atoms as MD does, we homogenize atoms in GDP molecule and tubulins and then represent them by a volume density ρ_i, number of atoms per unit volume before deformation, where the subscript "i" denotes the type of atoms, which can be carbon (C), hydrogen (H), oxygen (O), phosphorus (P), and sulfur (S). Using this notation, for example, the number of C atoms in GDP molecule over the volume dV_G is $\rho_G^C dV_G$, where the subscript "G" denotes GDP molecule and the superscript "C" denotes carbon atom. Since the atomic structures and molecular formulas of α- and β-tubulins are very similar,

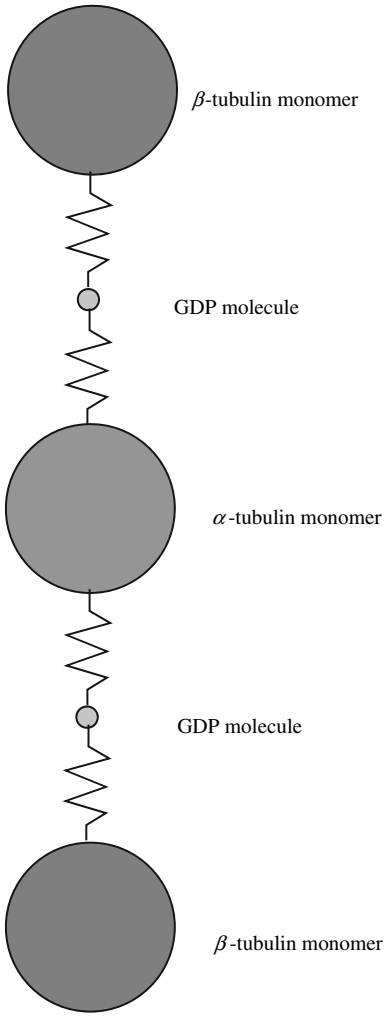

Fig. 2 A one-dimensional chain model for a protofilament, formed by three rigid bodies connected with nonlinear springs. The three rigid bodies represent α-tubulin, β-tubulin, and GDP molecule; and the nonlinear spring denotes the interface between GDP molecule and tubulin

we ignore their difference here and use the same volume and volume density for each type of atoms. Thus the number of H atoms for example in a tubulin over the volume dV_t is $\rho_t^H dV_t$, where the subscript "t" denotes tubulin. We first proposed this homogenization method to establish a cohesive law for carbon nanotube/polymer composites [50]. We proved that the results by homogenization method through the volume density are the same as those by direct summation over discrete atoms for strictly periodic structures, which can be found in the Appendix of reference [50]. Although the α-tubulin, β-tubulin, and GDP molecules do not have strictly periodic structures, their large numbers of atoms ensure that the homogenization method is applicable from a statistic point of view. Due to the necessity of electroneutrality, the electrostatic interactions are ignored because of the homogenization.

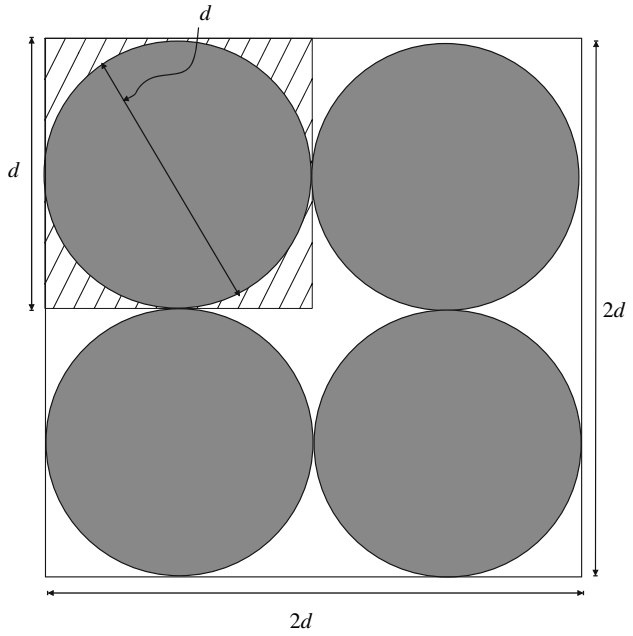

Fig. 3 A two dimensional atomic system with four tightly packed atoms of identical diameter d. The *shaded region* is the area occupied by a single atom

When homogenizing the discrete atoms as a volume density, we need to differentiate between the solid volume and the volume that the atoms occupy in space, namely space volume. For instance, Fig. 3 illustrates a two-dimensional atomic system with four tightly packed atoms with identical diameter d. The solid area that each atom has is $\pi d^2/4$, while the area this atom occupies (also the area for homogenization or space area) is $d \times d$. This is because in homogenization the discrete atoms are replaced by a uniform volume density, i.e., the atoms are assumed to be distributed evenly and fill the *entire* space in homogenization. Since a microtubule consists of 13 protofilaments (cross section is shown in Fig. 4a) where the outer and inner radius are $r_{\text{outer}} = 12.5\,\text{nm}$ and $r_{\text{inner}} = 7.7\,\text{nm}$, respectively, the area that those 13 protofilaments occupy in space is an annulus with area of $\pi\left(r_{\text{outer}}^2 - r_{\text{inner}}^2\right)$. Then the shaded annular sector is the area that one α- or β-tubulin occupies in the cross section and given by $\frac{\pi}{13}\left(r_{\text{outer}}^2 - r_{\text{inner}}^2\right)$. Therefore the space volume that one tubulin occupies is a slice of an annular structure as shown Fig. 4b. The space volume for one tubulin monomer is then given as $V_t = \frac{\pi}{13}\left(r_{\text{outer}}^2 - r_{\text{inner}}^2\right)D = 113.6\,\text{nm}^3$, where D (=4.8 nm) is the diameter of one tubulin. Similarly, the space volume for one GDP molecule is given by $V_G = \frac{\pi}{13}\left(r_{\text{outer}}^2 - r_{\text{inner}}^2\right)H = 12.9\,\text{nm}^3$, where H (=0.55 nm) is the height of a GDP molecule. Since the height of a GDP molecule ($H = 0.55\,\text{nm}$) is one order of magnitude smaller than the height of a tubulin monomer ($D = 4.8\,\text{nm}$), we further model the tubulin monomer as an infinite body and the GDP as a two-dimensional sheet with vanishing thickness, as shown in Fig. 5a. Once the volume is determined, the volume densities of all type of atoms are obtained based on chemical formulas. Table 1 provides all the parameters for microtubules, including the parameters of the atomistic potential and the volume densities of all type of atoms in tubulin monomer and GDP molecule.

Without losing generality, we choose one C atom as the origin in GDP two-dimensional sheet. We use h_0 to denote the

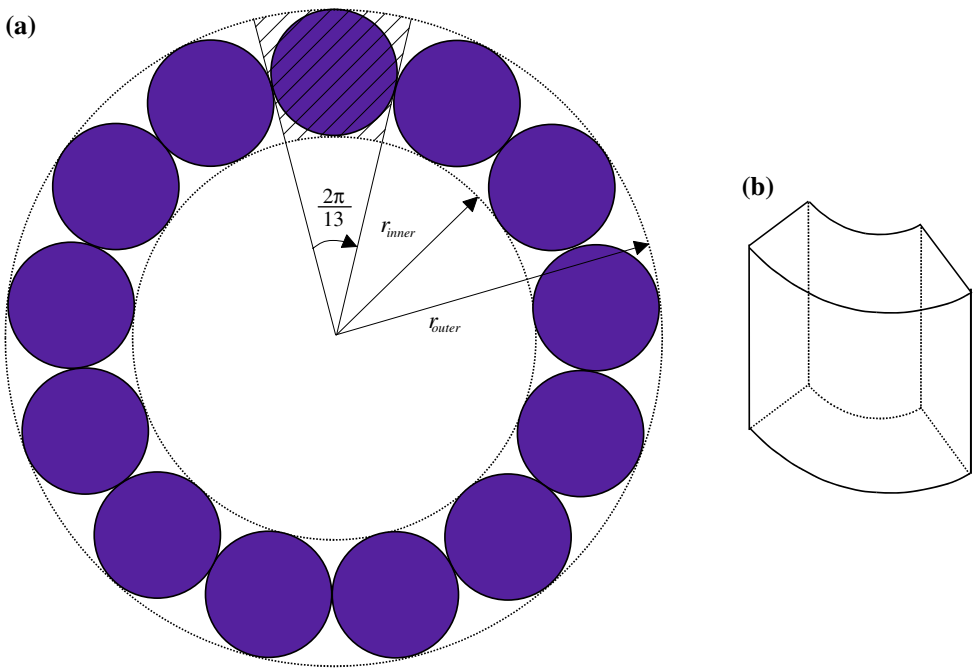

Fig. 4 **a** The cross section of a microtubule with 13 protofilaments, where $r_{\text{outer}} = 12.5\,\text{nm}$ and $r_{\text{inner}} = 7.7\,\text{nm}$ are outer and inner radius for a microtubule, respectively, and $\frac{2\pi}{13}$ is the annular angle of one tubulin. The *shaded annular sector* is the area one α- or β-tubulin occupies in the cross section. **b** The volume of one α- or β-tubulin occupies in space, namely, space volume, which is also the volume used in homogenization

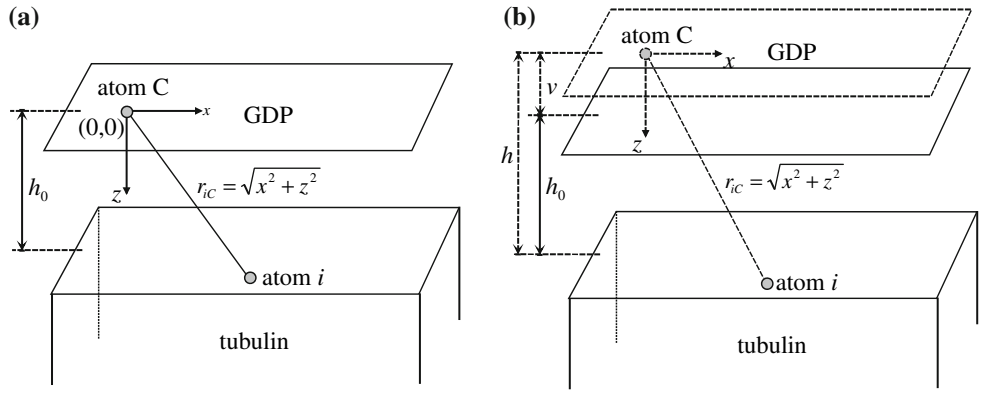

Fig. 5 A schematic diagram of a two-dimensional GDP sheet parallel to the surface of an infinite tubulin: **a** the equilibrium spacing between the GDP sheet and tubulin surface is h_0, x and z denote the radial distance and vertical distance between one C atom in GDP molecule and another atom in tubulin, respectively; **b** the two-dimensional GDP sheet is subjected to the opening displacement v due to external loading in axial direction of protofilament. h is the new spacing between the GDP sheet and tubulin surface

Table 1 Parameters for the microtubules calculation

(a) ε_{ij} for tubulin monomer and GDP molecule

ε_{ij} (kcal/mol)		Tubulin				
		C	H	N	O	S
GDP	C	0.1094	0.04144	0.1364	0.1516	0.1654
	H	0.04144	0.01570	0.05166	0.05742	0.06265
	N	0.1364	0.05166	0.1700	0.1889	0.2062
	O	0.1516	0.05742	0.1889	0.2100	0.2291
	P	0.1479	0.05604	0.1844	0.2049	0.2236

(b) σ_{ij} for tubulin monomer and GDP molecule

σ_{ij} (nm)		Tubulin				
		C	H	N	O	S
GDP	C	0.3816	0.3308	0.3732	0.3569	0.3908
	H	0.3308	0.2800	0.3224	0.3061	0.3400
	N	0.3732	0.3224	0.3648	0.3485	0.3824
	O	0.3569	0.3061	0.3485	0.3322	0.3661
	P	0.4008	0.3500	0.3924	0.3761	0.4100

(c) Volume density for all type of atoms in tubulin and GDP molecule

$\rho(/\text{nm}^3)$	C	H	N	O	S	P
Tubulin	19.07	37.10	5.026	9.444	0.3961	–
GDP	0.7726	1.159	0.3863	0.8498	–	0.1545

The data in table are from Cornell et al. [48]

initial equilibrium spacing between the infinite body (tubulin) and two-dimensional sheet (GDP molecule). The distance between this C atom and another atom i in tubulin is $r_{iC} = \sqrt{x^2 + z^2}$, where x and z denote the radial distance and vertical distance between C atom and i atom, respectively. Atom i in tubulin can be any type of atoms in tubulin, including C, H, O, N, and S. For the infinitesimal volume dV_G of GDP molecule, the energy stored due to non-bonded energies between C atoms of GDP and atom i of tubulin is given by $\rho_G^C dV_G \left[\int_V U(r_{iC}) \rho_t^i dV_t \right]$. Because of homogenization, r_{iC} varies continuously so that the integration is used instead of

summation over discrete atoms in a tubulin monomer. Since atom i can be any type of atoms in tubulin, the total interaction between C atoms in dV_G and other atoms in tubulin is given by the summation over all types of atoms in tubulin, i.e.,

$$dW_G^C = \rho_G^C dV_G \left[\sum_{i=C,H}^{N,O,S} \int_V U(r_{iC}) \rho_t^i dV_t \right] = 2\pi \rho_G^C dV_G \left[\sum_{i=C,H}^{N,O,S} \rho_t^i \int_{z=h_0}^{\infty} dz \int_{x=0}^{\infty} U(r_{iC}) x dx \right]. \quad (3)$$

Substitute the non-bonded energies Eq. 2 into Eq. 3, the total non-bonded energies between C atoms of GDP and the entire tubulin in the infinitesimal volume dV_G of the GDP is given by

$$dW_G^C = \frac{4\pi}{3} \rho_G^C dV_G \left[\sum_{i=C,H}^{N,O,S} \rho_t^i \varepsilon_{iC} \left(\frac{\sigma_{iC}^{12}}{15 h_0^9} - \frac{\sigma_{iC}^6}{2 h_0^3} \right) \right], \quad (4)$$

where, ε_{iC} and σ_{iC} are parameters in non-bonded energies for atom i and atom C, given by Cornell et al. [48]. Similarly, the non-bonded energies between other atoms in GDP and the entire tubulin can also be obtained. Then the total interaction between an infinitesimal GDP volume dV_G and the entire tubulin molecule is

$$dW_G = \frac{4\pi}{3} \sum_{j=C,H}^{N,O,P} \rho_G^j \left[\sum_{i=C,H}^{N,O,S} \rho_t^i \varepsilon_{ij} \left(\frac{\sigma_{ij}^{12}}{15 h_0^9} - \frac{\sigma_{ij}^6}{2 h_0^3} \right) \right] dV_G. \quad (5)$$

The cohesive energy Φ is the energy per unit volume, and is thus given by

$$\Phi = \frac{4\pi}{3} \sum_{j=C,H}^{N,O,P} \rho_G^j \left[\sum_{i=C,H}^{N,O,S} \rho_t^i \varepsilon_{ij} \left(\frac{\sigma_{ij}^{12}}{15 h_0^9} - \frac{\sigma_{ij}^6}{2 h_0^3} \right) \right], = \frac{2\pi}{3} \left(\frac{A}{h_0^9} - \frac{B}{h_0^3} \right), \quad (6)$$

where A and B are

$$A = \frac{2}{15} \sum_{j=C,H}^{N,O,P} \rho_G^j \sum_{i=C,H}^{N,O,S} \rho_t^i \varepsilon_{ij} \sigma_{ij}^{12} = 2.43 \times 10^{-6} \text{ kcal/mol nm}^6$$
$$B = \sum_{j=C,H}^{N,O,P} \rho_G^j \sum_{i=C,H}^{N,O,S} \rho_t^i \varepsilon_{ij} \sigma_{ij}^6 = 0.016 \text{ kcal/mol}. \quad (7)$$

Remarkably, A and B are not fitting parameters, rather they are directly related to the non-bonded energies and the volume density of atoms.

We determine the initial equilibrium distance to be $h_0 = (3A/B)^{1/6} = 0.28$ nm by minimizing the energy by setting $\partial\Phi/\partial h_0 = 0$. When the microtubule is subject to applied axial loading, it will deform in this direction with certain opening displacement v (Fig. 5b). The Green strain, which describes the strain for finite deformation, is given by [51]

$$E_{11} = \frac{1}{2} \left[2\frac{v}{h_0} + \left(\frac{v}{h_0} \right)^2 \right]. \quad (8)$$

Then the new spacing h between GDP molecule and tubulin becomes

$$h = h_0 \sqrt{1 + 2E_{11}}. \quad (9)$$

The cohesive energy can be similarly obtained as

$$\Phi = \frac{2\pi}{3} \left[\frac{A}{h_0^9 (1 + 2E_{11})^{9/2}} - \frac{B}{h_0^3 (1 + 2E_{11})^{3/2}} \right]. \quad (10)$$

Then the tensile cohesive stress (second Piola–Kirchhoff stress [51]), is the work conjugate with Green strain E_{11} and is obtained as

$$T_{\text{cohesive}} = \frac{\partial \Phi}{\partial E_{11}} = 2\pi \left[\frac{B}{h_0^3 (1 + 2E_{11})^{5/2}} - \frac{3A}{h_0^9 (1 + 2E_{11})^{11/2}} \right], \quad (11)$$

and the axial incremental modulus is given by

$$C = \frac{\partial T_{\text{cohesive}}}{\partial E_{11}} = 2\pi \left[\frac{33A}{h_0^9 (1 + 2E_{11})^{13/2}} - \frac{5B}{h_0^3 (1 + 2E_{11})^{7/2}} \right]. \quad (12)$$

Equations 11 and 12 provide the continuum constitutive relation and the incremental modulus for each individual protofilament.

Perpendicular to the axial direction, neighboring protofilaments have lateral interactions, mainly through monomers of the same type (α–α and β–β). Biological studies have shown that the interactions holding α and β monomers through GDP molecule are stronger than interactions between the same type monomers. From the mechanics point of view, it is because the initial equilibrium spacing between two infinite bodies (monomers of the same type, α–α or β–β) is larger than spacing between an infinity body (α- or β-tubulin monomer) and a two-dimensional sheet (GDP molecule). With the increase of spacing, the cohesive energy quickly decreases, such that the interaction between the same type monomers is weaker than that holding α and β monomers through GDP molecule. Therefore, we ignore the interactions between different protofilaments, though the interactions between different protofilaments might be important for compression. This will be examined in future work.

The axial stress and modulus of an individual microtubule is the sum of 13 protofilaments,

$$T_{\text{cohesive}} = 26\pi\left[\frac{B}{h_0^3(1+2E_{11})^{5/2}} - \frac{3A}{h_0^9(1+2E_{11})^{11/2}}\right], \tag{13}$$

$$C = \frac{\partial T_{\text{cohesive}}}{\partial E_{11}} = 26\pi\left[\frac{33A}{h_0^9(1+2E_{11})^{13/2}} - \frac{5B}{h_0^3(1+2E_{11})^{7/2}}\right]. \tag{14}$$

In the development of this continuum constitutive relation for microtubules, we do not introduce any fitting parameters, but simply follow the interatomic potential developed for protein [48] and the atomistic structures of microtubules.

4.2 Example: elastic modulus and bending rigidity of microtubules

The direct experimental measurements of mechanical properties of CSK biopolymer network have fascinated scientists for decades; previous studies were highlighted in Sect. 1. In this section, the elastic modulus and bending rigidity of microtubules will be calculated analytically based on the developed continuum constitutive relation for microtubules.

The elastic modulus is defined as the axial incremental modulus at small strain, i.e.,

$$Y = C(E_{11}=0) = 26\pi\left(\frac{33A}{h_0^9} - \frac{5B}{h_0^3}\right) = 52\sqrt{3}\pi\sqrt{\frac{B^3}{A}} = 2.65\,\text{GPa}. \tag{15}$$

This value $Y = 2.65$ GPa solely depends on the non-bonded energies given by Cornell et al. [48] and the atomic structure of microtubule. The *elastic modulus* $Y = 2.65$ GPa *agrees satisfactorily with the range of experimentally measured value of* (1–2.55 GPa) [17,18] *without any parameter fitting*.

The bending rigidity of microtubules is given by

$$EI = Y\frac{\pi}{4}\left(r_{\text{outer}}^4 - r_{\text{inner}}^4\right) = 4.3\times10^{-23}\,\text{N m}^2. \tag{16}$$

This value agrees well with the range of experimentally measured value of (2–4.4 $\times 10^{-23}$ N m^2) [52] without any parameter fitting.

4.3 Example: stress–strain relations in finite tensile deformation

Equation (13) provides a general stress–strain relation for finite deformation, which is more important than the elastic modulus since the nonlinear nature of biological systems. To our best knowledge, all existing experimental measurements on CSK filaments are focused on the elastic modulus and there does not have experimental measurements of strain–strain relation for a certain range of deformation. Therefore the current study provides a complementary analysis to experiments. We also need to point out that since the current method ignores the interactions between neighboring protofilaments that might be important to compression; the stress-strain relation in this section is only for finite tensile strain.

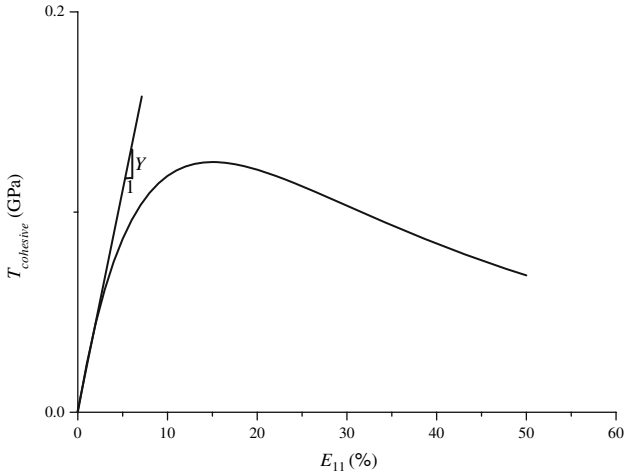

Fig. 6 Cohesive stress T_{cohesive} and axial strain E_{11} relation in finite deformation

Figure 6 shows the cohesive stress T_{cohesive} (Eq. 13) versus the axial tensile strain E_{11}. These large deformations are in line with strains exerted on the CSK in vivo. The peak of the curve ($T_{\text{cohseive}} = 0.12$ GPa) occurs at 17% axial strain, which corresponds to the strength of the microtubules, i.e., the maximum stress the microtubules can exert. A strong nonlinear effect is observed, where the elastic modulus given by Sect. 4.2 only corresponds to the slope of the curve at zero axial strain. With the increasing of the axial tensile strain, the slop of the curve decreases, which represents the gradual softening effect of microtubules.

5 Discussion and concluding remarks

We have developed an atomistic-based continuum constitutive relation for microtubules based on the interatomic potential for proteins and homogenization method. Both the constitutive relation and incremental modulus are in the framework of finite deformation, which enables large deformation, similar to those experienced by living cells, to be probed. This theory has been applied to calculate the elastic modulus of microtubules which falls in the range of experiments without any fitting parameters. The elastic modulus is

slightly overestimated, which we attribute to modeling each tubulin molecule as a rigid body and restrict the deformation inside each tubulin. This restriction confines the free movement of atoms in tubulin molecule and thus makes the entire microtubule stiffer. Some other aspects in the theory will be discussed in the following.

Homogenization: in terms of homogenization method used in this paper, it is applicable to three-dimensional solids, two-dimensional plates, or even fractal dimension objects. The most important point for homogenization is to determine the volume/area that the subject occupies. However, the determination of the volume for subjects with fractal dimension less than 3 is not straightforward and depends on the specific situations. The accuracy of homogenization needs to be further justified for other biological system, although it has been proved mathematically to be as accurate as following each individual atom if the object has strictly periodic structure [53].

Water molecule and temperature effect: although the model has no explicit water molecules involved, the theory as applied implicitly includes the influence of water molecules. It is well known that cells or biopolymers exhibit different conformation with or without water environment. In other words, the atomic structure of CSK filament strongly depends on water molecules. The theory developed in this paper is based on atomic information, including the atomic structures and interatomic potentials, such that the water molecules do come into the theory through the atomic structure of biopolymers. Specifically for microtubules, the atomic structures used in modeling are obtained from the Protein Data Bank that already takes into account the water molecules.

The same arguments also hold for temperature effect. The temperature was specified as liquid-nitrogen temperature in the electron microscope observation for tubulin monomers used in this study [54], which is indeed the data source for the tubulin monomer (1TUB) in the Protein Data Bank. Therefore, temperature effect also plays a role in the theory via the atomic structure.

Generality of the current method: although the proposed method is only used for one type of CSK filaments, microtubules, *it provides a possible route to study other biopolymers if the monomers are bonded together through noncovalent bonds*. Without tracking each individual atom, the homogenization method through volume density satisfactorily reproduces the elastic modulus and bending rigidity of microtubules and predicts the stress-strain relation that is not accessible by current experimental techniques. The examples in Sects. 4.2 and 4.3 serve as benchmarks for the proposed method to ensure the applicability to other biopolymers with non-covalently bonded monomers. In fact, many biopolymer monomers are non-covalently bonded because they polymerize and depolymerize to fulfill some biological functions. For instance, another type of CSK filaments, actin filament has a similar structure to microtubules. Like tubulin, each actin monomer has a binding site for a nucleotide adenosine triphosphate (ATP) or adenosine diphosphate (ADP). Actin monomers then assemble head-to-tail through *non-covalent bonds* to form filaments. Like α- and β-tubulins bonded through GDP molecule, actin filaments are cross-linked and bonded together by a variety of accessory proteins.

Static theory and CSK dynamic reorganization: although the developed atomistic-based continuum theory is a static theory, it forms the basis to study the CSK dynamic reorganization. Specifically for microtubules, there have been extensive studies about microtubules reorganization and its dependence on tubulin monomer concentration and other regulatory factors [55–59]. Therefore, from the continuum point of view, another theory (multiscale biomechanics theory warping from nanoscale to microscale) is currently being developed to model the CSK reorganization via a state variable that depends on the monomer concentration and other regulatory factors. While, this paper, the elastic modulus of each microtubules, serves as the atomic-scale modeling and provides the input for the microscale cell mechanics. Thus this study takes a coherent role in a multiscale approach to study the CSK reorganization with atomic-scale information as input. This theory also bridges continuum mechanics and molecular dynamic simulations to provide molecular insight into macroscopic mechanical properties and enables multiscale modeling to predict difficult to measure properties of biological constructs.

Acknowledgments HJ, JDP, BDV acknowledge the financial support from the Fulton School of Engineering at ASU. LY acknowledges the support from NSERC. HJ acknowledges the partial support from NSF CMMI-0700440. BDV acknowledges the partial support from NSF CMMI-0653989.

References

1. Alberts B, Johnson A, Lewis J, Raff M, Roberts K, Walter P (2003) Molecular Biology of the Cell. Garland
2. Suresh S (2006) Mechanical response of human red blood cells in health and disease: some structure property–function relationships. J Mater Res 21:1871–1877
3. Suresh S, Spatz J, Mills JP, Micoulet A, Dao M, Lim CT, Beil M, Seufferlein T (2005) Connections between single-cell biomechanics and human disease states: gastrointestinal cancer and malaria. Acta Biomater 1:15–30
4. Stamenovic D, Mijailovich SM, Tolic-Norrelykke IM, Chen JX, Wang N (2002) Cell prestress. II. Contribution of microtubules. Am J Physiol Cell Physiol 282:C617–C624
5. Ingber DE (1993) Cellular tensegrity—defining new rules of biological design that govern the cytoskeleton. J Cell Sci 104:613–627
6. Wang N, Stamenovic D (2000) Contribution of intermediate filaments to cell stiffness, stiffening, and growth. Am J Physiol Cell Physiol 279:C188–C194
7. Sato M, Schwartz WH, Selden C, Pollard TD (1988) Mechanical properties of brain tubulin and microtubules. J Cell Biol 106:1205–1211

8. Sato M, Leimbach G, Schwarz WH, Pollard TD (1985) Mechanical properties of actin. J Cell Biol 260:8585–8592
9. Kurachi M, Hoshi M, Tashiro H (1995) Buckling of a single microtubule by optical trapping forces—direct measurement of microtubule rigidity. Cell Motil Cytoskeleton 30:221–228
10. Takasone T, Juodkazis S, Kawagishi Y, Yamaguchi A, Matsuo S, Sakakibara H, Nakayama H, Misawa H (2002) Flexural rigidity of a single microtubule. Jpn J Appl Phys Part 1-Regular Papers Short Notes & Review Papers 41:3015–3019
11. Elbaum M, Fygenson DK, Libchaber A (1996) Buckling microtubules in vesicles. Phys Rev Lett 76:4078–4081
12. Fygenson DK, Elbaum M, Shraiman B, Libchaber A (1997) Microtubules and vesicles under controlled tension. Phys Rev E 55:850–859
13. Fygenson DK, Flyvbjerg H, Sneppen K, Libchaber A, Leibler S (1995) Spontaneous nucleation of microtubules. Phys Rev E 51:5058–5063
14. Kis A, Kasas S, Babic B, Kulik AJ, Benoit W, Briggs GAD, Schonenberger C, Catsicas S, Forro L (2002) Nanomechanics of microtubules. Phys Rev Lett 89:248101
15. Chaudhuri O, Parekh SH, Fletcher DA (2007) Reversible stress softening of actin networks. Nat Mater 445:295–298
16. Mizuno D, Tardin C, Schmidt CF, MacKinstosh FC (2007) Nonequilibrium mechanics of active cytoskeletal networks. Science 315:370–373
17. Wagner O, Zinke J, Dancker P, Grill W, Bereiter-Hahn J (1999) Viscoelastic properties of f-actin, microtubules, f-actin/alpha-actinin, and f-actin/hexokinase determined in microliter volumes with a novel nondestructive method. Biophys J 76:2784–2796
18. Pablo PJde , Schaap IAT, MacKintosh FC, Schmidt CF (2003) Deformation and collapse of microtubules on the nanometer scale. Phys Rev Lett 91:4
19. Brooks BR, Bruccoleri RE, Olafson BD, States DJ, Swaminathan S, Karplus M (1983) Charmm—a program for macromolecular energy, minimization, and dynamics calculations. J Comput Chem 4:187–217
20. Weiner PK, Kollman PA (1981) Amber—assisted model-building with energy refinement—a general program for modeling molecules and their interactions. J Comput Chem 2:287–303
21. Duan Y, Kollman PA (1998) Pathways to a protein folding intermediate observed in a 1-μs simulation in aqueous solution. Science 282:740–744
22. Weber W, Helms V, McCammon JA, Langhoff PW (1999) Shedding light on the dark and weakly fluorescent states of green fluorescent proteins. Proc Natl Acad Sci USA 96:6177–6182
23. Chu JW, Voth GA (2006) Coarse-grained modeling of the actin filament derived from atomistic-scale simulations. Biophys J 90:1572–1582
24. Chu JW, Voth GA (2005) Allostery of actin filaments: molecular dynamics simulations and coarse-grained analysis. Proc Natl Acad Sci USA 102:13111–13116
25. Wang YL (1984) Reorganization of actin filament bundles in living fibroblasts. J Cell Biol 99:1478–1485
26. Stamenovic D, Ingber DE (2002) Models of cytoskeletal mechanics of adherent cells. Biomech Model Mechanobiol 1:95–108
27. Janosi IM, Chretien D, Flyvbjerg H (1998) Modeling elastic properties of microtubule tips and walls. Eur Biophys J Biophys Lett 27:501–513
28. Nishimura S, Nagai S, Katoh M, Yamashita H, Saeki Y, Okada J, Hisada T, Nagai R, Sugiura S (2006) Microtubules modulate the stiffness of cardiomyocytes against shear stress. Circ Res 98: 81–87
29. Wada H, Netz RR (2006) Non-equilibrium hydrodynamics of a rotating filament. Europhys Lett 75:645–651
30. Stamenovic D, Wang N (2000) Invited review: engineering approaches to cytoskeletal mechanics. J Appl Physiol 89:2085–2090
31. Stamenovic D, Coughlin MF (1999) The role of prestress and architecture of the cytoskeleton and deformability of cytoskeletal filaments in mechanics of adherent cells: a quantitative analysis. J Theor Biol 201:63–74
32. Sultan C, Stamenovic D, Ingber DE (2004) A computational tensegrity model predicts dynamic rheological behaviors in living cells. Ann Biomed Eng 32:520–530
33. Liu WK, Liu YL, Farrell D, Zhang L, Wang XS, Fukui Y, Patankar N, Zhang YJ, Bajaj C, Lee J, Hong JH, Chen XY, Hsu HY (2006) Immersed finite element method and its applications to biological systems. Comput Meth Appl Mech Eng 195:1722–1749
34. Boey SK, Boal DH, Discher DE (1998) Simulations of the erythrocyte cytoskeleton at large deformation. I. Microscopic models. Biophys J 75:1573–1583
35. Tadmor EB, Ortiz M, Phillips R (1996) Quasicontinuum analysis of defects in solids. Philos Mag Phys Condens Matter Struct Defects Mech Prop 73:1529–1563
36. Tadmor EB, Phillips R, Ortiz M (1996) Mixed atomistic and continuum models of deformation in solids. Langmuir 12:4529–4534
37. Miller R, Tadmor EB, Phillips R, Ortiz M (1998) Quasicontinuum simulation of fracture at the atomic scale. Modell Simul Mater Sci Eng 6:607–638
38. Shenoy VB, Miller R, Tadmor EB, Phillips R, Ortiz M (1998) Quasicontinuum models of interfacial structure and deformation. Phys Rev Lett 80:742–745
39. Shenoy VB, Miller R, Tadmor EB, Rodney D, Phillips R, Ortiz M (1999) An adaptive finite element approach to atomic-scale mechanics—the quasicontinuum method. J Mech Phys Solids 47:611–642
40. Friesecke G, James RD (2000) A scheme for the passage from atomic to continuum theory for thin films, nanotubes and nanorods. J Mech Phys Solids 48:1519–1540
41. Arroyo M, Belytschko T (2002) An atomistic-based finite deformation membrane for single layer crystalline films. J Mech Phys Solids 50:1941–1977
42. Xiao SP, Yang WX (2007) A temperature-related homogenization technique and its implementation in the meshfree particle method for nanoscale simulations. Int J Numer Methods Eng 69:2099–2125
43. Xiao SP, Yang WX (2006) Temperature-related Cauchy–Born rule for multiscale modeling of crystalline solids. Comput Mater Sci 37:374–379
44. Chung PW, Narnburu RR (2003) On a formulation for a multiscale atomistic-continuum homogenization method. Int J Solids Struct 40:2563–2588
45. Jiang H, Huang Y, Hwang KC (2007) Mechanics of carbon nanotubes: a continuum theory based on interatomic potentials. Key Eng Mater 340(341):11–20
46. Jiang H, Zhang P, Liu B, Huang Y, Geubelle PH, Gao H, Hwang KC (2003) The effect of nanotube radius on the constitutive model for carbon nanotubes. Comput Mater Sci 28:429–442
47. Zhang P, Jiang H, Huang Y, Geubelle PH, Hwang KC (2004) An atomistic-based continuum theory for carbon nanotubes: analysis of fracture nucleation. J Mech Phys Solids 52:977–998
48. Cornell WD, Cieplak P, Bayly CI, Gould IR, Merz KM, Ferguson DM, Spellmeyer DC, Fox T, Caldwell JW, Kollman PA (1995) A 2nd generation force-field for the simulation of proteins, nucleic-acids, and organic-molecules. J Am Chem Soc 117:5179–5197
49. Chretien D, Metoz F, Verde F, Karsenti E, Wade RH (1992) Lattice-defects in microtubules—protofilament numbers vary within individual microtubules. J Cell Biol 117:1031–1040

50. Jiang LY, Huang Y, Jiang H, Ravichandran G, Gao H, Hwang KC, Liu B (2006) A cohesive law for carbon nanotube/polymer interfaces based on the van der Waals force. J Mech Phys Solids 54:2436–2452
51. Symon K (1971) Mechanics. Addison-Wesley, Reading
52. Gittes F, Mickey B, Nettleton J, Howard J (1993) Flexural rigidity of microtubules and actin-filaments measured from thermal fluctuations in shape. J Cell Biol 120:923–934
53. Jiang H, Huang Y, Hwang KC (2005) A finite-temperature continuum theory based on interatomic potentials. J Eng Mater Technol Trans ASME 127:408–416
54. Nogales E, Wolf SG, Downing KH (1998) Structure of the alpha beta tubulin dimer by electron crystallography. Nature 391:199–203
55. Desai A, Mitchison TJ (1997) Microtubule polymerization dynamics. Annu Rev Cell Dev Biol 13:83–117
56. Walker RA, Pryer NK, Salmon ED (1991) Dilution of individual microtubules observed in real-time in vitro—evidence that cap size is small and independent of elongation rate. J Cell Biol 114: 73–81
57. Walker RA, Obrien ET, Pryer NK, Soboeiro MF, Voter WA, Erickson HP, Salmon ED (1988) Dynamic instability of individual microtubules analyzed by video light-microscopy—rate constants and transition frequencies. J Cell Biol 107:1437–1448
58. Fygenson DK, Braun E, Libchaber A (1994) Phase-diagram of microtubules. Phys Rev E 50:1579–1588
59. Kinoshita K, Arnal I, Desai A, Drechsel DN, Hyman AA (2001) Reconstitution of physiological microtubule dynamics using purified components. Science 294:1340–1343